The Crab Nebula's "Wisps" as Shocked Pulsar Wind

Yves A. Gallant, Jonathan Arons, and A. Bruce Langdon

Manuscript date: July 20, 1992

UCRL-JC-111254

Lawrence Livermore National Laboratory
University of California

UCRL-JC--111254

DE93 003466

The Crab Nebula's "Wisps" as Shocked Pulsar Wind

Yves A. Gallant[1,3], Jonathan Arons[1,3], and A. Bruce Langdon[2,3]

[1]Theoretical Astrophysics Center, Astronomy Department, U. C. Berkeley
[2]X-Division, Lawrence Livermore National Laboratory
[3]Institute for Geophysics and Planetary Physics, LLNL

1 INTRODUCTION: RELATIVISTIC, COLLISIONLESS SHOCKS

The Crab synchrotron nebula has been successfully modelled as the post-shock region of a relativistic, magnetized wind carrying most of the spindown luminosity from the central pulsar (Rees and Gunn 1974, Kundt and Krotscheck 1980, Kennel and Coroniti 1984a,b, Emmering and Chevalier 1987). While the Crab is the best-studied example, most of the highest spindown luminosity pulsars are also surrounded by extended synchrotron nebulae, and several additional supernova remnants with "plerionic" morphologies similar to the Crab are known where the central object is not seen (Weiler 1985, Helfand and Becker 1987, Weiler and Sramek 1988). All these objects have nonthermal, power-law spectra attributable to accelerated high-energy particles thought to originate in a Crab-like relativistic pulsar wind. However, proposed models have so far treated the wind shock as an infinitesimally thin discontinuity, with an arbitrarily ascribed particle acceleration efficiency. To make further progress, investigations resolving the shock structure seemed in order.

Motivated by these considerations, we have performed "particle-in-cell" (PIC) simulations of perpendicularly magnetized shocks in electron-positron and electron-positron-ion plasmas (see Arons *et al.*, these proceedings). The shocks in pure electron-positron plasmas were found to produce only thermal distributions downstream, and are thus poor candidates as particle acceleration sites. When the upstream plasma flow also contained a smaller population of positive ions, however, efficient acceleration of positrons, and to a lesser extent of electrons, was observed in the simulations.

Figure 1 displays the structure of such a electron-positron-ion shock, in the case where most of the upstream energy is in the bulk flow of the ions. The shock structure is characterized by two length scales: the electrons and positrons are first magnetically reflected and thermalized on a length scale on the order of their Larmor radius, $r_{L\pm} = m_e \gamma_1 c^2/(eB_1)$, where B_1 and γ_1 are the upstream perpendicular magnetic field and flow Lorentz factor, respectively. This "pair shock" is entirely analogous to the shock structure observed in pure pair plasmas (Gallant *et al.* 1992), as the background ion flow is essentially unaffected on this length scale.

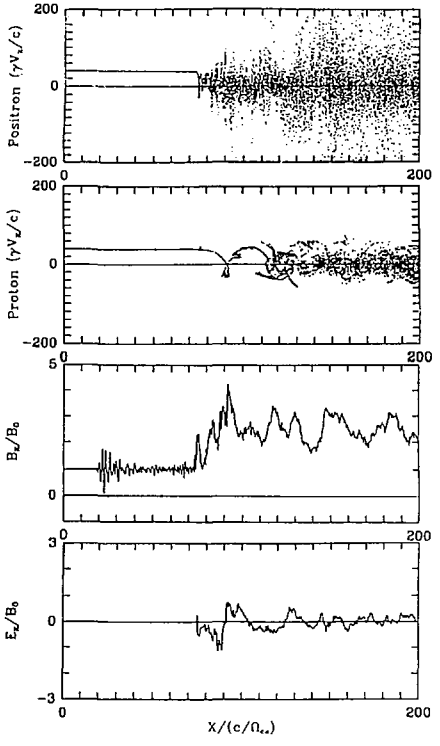

Fig. 1 — Structure of an electron-positron-ion shock as revealed by simulations (Hoshino *et al.* 1992). The top two panels display u_x vs x phase space for the positrons and the ions, respectively, while the lower two panels show the magnetic and electrostatic fields. Shock parameters (definitions in §4) were $1/\sigma_i = 2$, $1/\sigma_\pm = 0.9$, and $\gamma_1 = 40$. The unit of length used for the x–axis is $r_{L\pm}$, corresponding to $r_{Li}/20$.

The ions are then reflected in turn, through a combination of magnetic reflection and electrostatic pull of the charged pair fluid, on a much larger length scale of order the ion Larmor radius, $r_{Li} = Am_p\gamma_1 c^2/(ZeB_1)$, where Ze and Am_p are the ion charge and mass, respectively. The downstream dissipation of this ion gyrational energy yields an acceleration of the pairs to power-law distributions, with an efficiency that can reach $\sim$ 20% of total wind energy available upstream (Hoshino *et al.* 1992). The increasing number of high-energy positrons downstream can clearly be observed in Figure 1. This acceleration process can be explained as coherent synchrotron emission from the initial ion loop followed by resonant absorption of these waves by the positrons and electrons (Hoshino and Arons 1991).

2 RESOLVED SHOCK STRUCTURE AND THE "WISPS"

One can show that for the parameters of the Crab pulsar's wind, as inferred by Kennel and Coroniti (1984a) or Emmering and Chevalier (1987), the global shock length scale, the ion Larmor radius, is in fact macroscopically large:

$$r_{Li} \approx 0.01 \left(\frac{A}{Z}\right) \left(\frac{\gamma_1}{10^6}\right) \left(\frac{10^{-4}\,\mathrm{G}}{B_1}\right) \mathrm{pc}, \qquad (1)$$

where 0.01 pc corresponds to an angular size of 1″ at the Crab distance of 2 kpc. Thus unlike almost all other astrophysical shocks, the shock terminating the Crab pulsar's wind is expected to exhibit an observationally resolvable structure.

The Crab synchrotron nebula has long been known to have structure on precisely this length scale and at the expected distance from the pulsar, namely the "wisps" (Scargle 1969), originally described as "light ripples" (Lampland 1921). A modern, high-resolution CCD image of the wisps, obtained by van den Bergh and Pritchet (1989) at the CFHT, is shown in contour plot form in Figure 2. In addition to the well-known series of bright wisps beginning about 10″ to the northwest of the pulsar, one can clearly distinguish a faint wisp to the southeast of the pulsar, apparently a fainter counterpart of the main wisp to the northwest.

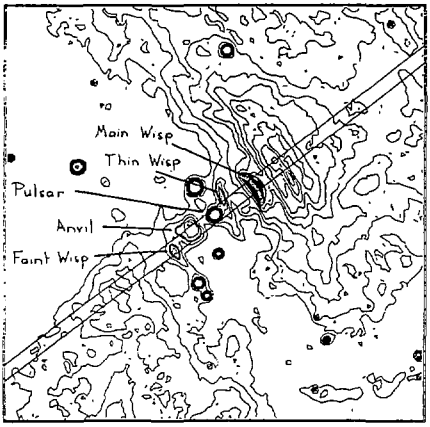

Fig. 2 — The central 1′ × 1′ of the Crab Nebula in continuum emission, showing the pulsar and the main wisp features, as identified by Scargle (1969), in his Figure 1*a*, except for the faint wisp. Contours are in equal flux intervals (arbitrary units) starting just above the "underluminous zone" flux level. From the I-band CCD data of van den Bergh and Pritchet (1989).

A cross-section along the pulsar-wisps axis of the average surface brightness from this image is shown in Figure 3. It can be seen that the wisps are local brightness enhancements superposed on the high brightness "plateau" to the northwest of the

pulsar. The dashed line represents the estimated foreground and background nebular emission, derived by assuming that the elliptical "underluminous zone" immediately surrounding the pulsar has negligible intrinsic emissivity (Kennel and Coroniti 1984a).

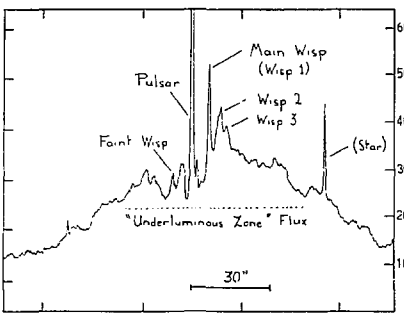

Fig. 3 — The brightness profile of the Crab Nebula along the pulsar-wisps axis: averaged flux above sky brightness (arbitrary units) for a strip 2″ wide centered on the pulsar and oriented at a position angle of −53° (drawn in outline across Figure 2). From the CCD data of van den Bergh and Pritchet (1989).

From the toroidal morphology of the X-ray emitting region in the Nebula, identified with the flow downstream of the shock, the wind is inferred to be mostly confined to the equatorial plane of the pulsar (Aschenbach and Brinkmann 1975; Brinkmann, Aschenbach and Langmeier 1985). Thus one would expect the shock to form a ring around the pulsar. The fact that wisps are seen only along the forward and backward flowing directions, i.e. along the two arcs of the ring where the magnetic field is perpendicular to the line of sight, can be partly explained by a combination of Doppler boosting and the anisotropy of the synchrotron emissivity, but probably also requires some underlying anisotropy in the synchrotron-emitting particle distribution. Polarization maps of the Crab Nebula (Michel *et al.* 1990) can also be interpreted as evidence for such anisotropy. In this context, investigations are under way to examine the growth and possible saturation of the Weibel instability, thought to be the dominant isotropization mechanism (see Yang *et al.*, these proceedings).

3 MODEL OF WISP EMISSION: SYNCHROTRON RADIATION FROM SHOCK-HEATED PAIRS

The brightness profile observed in Figure 3 is readily explained in terms of the collisionless shock structure as uncovered by our simulations: beyond the pair shock, the thermalized pairs will radiate synchrotron radiation with critical frequencies corresponding to Lorentz factors on the order of γ_1, i.e. around the optical waveband:

$$\nu_c \sim \frac{1}{2\pi}\frac{\gamma_1^2 eB_1}{m_e c} \approx 3\times 10^{14}\left(\frac{\gamma_1}{10^6}\right)^2\left(\frac{B_1}{10^{-4}\,\mathrm{G}}\right)\,\mathrm{Hz} \qquad (2)$$

Moreover, the synchrotron emissivity will correlate very strongly with the magnetic field. Consider the plane-parallel case for illustration: to a good approximation,

the pairs are frozen to the field lines, so that their number density $N_\pm$ scales as B. Then ignoring particle acceleration and radiative losses, average particle energies will be determined by adiabatic compression and expansion, i.e. $\gamma_\pm \propto B^{1/2}$ if the particles gyrate perpendicularly to the magnetic field and conserve their first adiabatic invariant, or $\gamma_\pm \propto B^{1/3}$ if they suffer rapid isotropization. Thus the total synchrotron power $P_{\rm synch}$ will scale as a high power of B:

$$P_{\rm synch} \propto N_\pm \gamma_\pm^2 B^2 \propto B^4 \text{ or } B^{11/3}, \tag{3}$$

where the two choices correspond to the extremes of no isotropization and complete isotropization. From Figure 1, it can be seen that the relativistic shock structure exhibits magnetic field enhancements in the ion reflection regions which can more than account for the observed brightness contrast of the wisps.

The proposed model is also entirely plausible on energetics grounds, as we now demonstrate. The synchrotron luminosity of the main wisp can be roughly estimated as the product of the total number of pairs emitted in the wind per unit time, $\dot{N}_\pm$, the time each particle spends in the first wisp region, roughly $r_{\rm L_i}/c$, and the single-particle sychrotron power, $\sigma_T c \gamma^2 B^2/4\pi$. If in addition we assume that essentially all the spindown energy of the Crab pulsar goes into the ion-dominated wind energy, i.e. $L_{\rm spindown} \approx \dot{N}_i m_i \gamma_1 c^2$, we obtain, using a neutron star moment of inertia of 10^{45} g cm^2,

$$L_{\rm wisp} \approx 5 \times 10^{33} \left(\frac{\gamma_1}{10^6}\right)^2 \left(\frac{B_1}{10^{-4}\,\rm G}\right) \left(\frac{\dot{N}_\pm/(Z\dot{N}_i)}{1000}\right) \text{ erg/s} \tag{4}$$

From this luminosity we can get an estimated flux in the I-band by assuming that the spectrum is roughly flat up to the critical frequency ν_c, and by factoring in the distance to the Crab:

$$F_\nu \sim \frac{5 \times 10^{33}\,\rm erg/s}{4\pi\,(2\,\rm kpc)^2}\,(3 \times 10^{14}\,\rm Hz)^{-1} \approx 4 \times 10^{-26}\,\rm erg/(cm^2\,s\,Hz). \tag{5}$$

The actual total flux from the main wisp, as measured from CCD image of van den Bergh and Pritchet (1989), is $(1.6\pm0.2)\times10^{-26}$ erg/(cm^2 s Hz) within the uncertainties due to background subtraction and nebular brightness calibration. Given the very approximate nature of the arguments leading to the above estimate, its agreement with the measured value is remarkably good.

4 "SOLITON" MODEL FOR THE SHOCK STRUCTURE

So that we may make quantitative comparisons of the observed brightness profile of the wisps with synchrotron emission from shocks with arbitrary values of the upstream wind parameters, we are developing a semi-analytical model of the shock structure on the ion Larmor radius scale. We treat the ions as remaining cold, while the pairs are represented as a hot, magnetized fluid past the pair shock. Since the

ions undergo no dissipation, this is analogous to a soliton model, except that we assume dissipation of the pairs' energy by imposing Rankine-Hugoniot conditions on the initial pair shock, which is treated as a discontinuous jump.

The main parameters of the upstream wind are the fractions of the incoming energy respectively invested in bulk flow of the ions, of the pairs, and in frozen-in Poyting flux, which we specify in terms of the two magnetization ratios σ_i and $\sigma_\pm$ for the ions and the pairs, respectively:

$$\frac{1}{\sigma_i} \equiv \frac{N_{1i} m_i \gamma_1 c^2}{B_1^2/4\pi} \quad \text{and} \quad \frac{1}{\sigma_\pm} \equiv \frac{N_{1\pm} m_\pm \gamma_1 c^2}{B_1^2/4\pi}, \tag{6}$$

with the subscript 1 indicating the upstream values. The upstream Lorentz factor γ_1 has negligible influence on the shock structure once $\gamma_1 \gg 1$, provided lengths are measured in units of the Larmor radius r_{Li}.

We seek a self-consistent solution for the ion orbit and the fields as a function of distance x behind the pair shock, with the ion equations of motion given by

$$\frac{d}{d(\Omega_{ci}\tau)}\left(\frac{x}{r_{Li}}\right) = \left(\frac{u_x}{u_1}\right) \tag{7}$$

$$\frac{d}{d(\Omega_{ci}\tau)}\left(\frac{u_x}{u_1}\right) = \left[\left(\frac{\gamma}{\gamma_1}\right)\left(\frac{E_x}{E_1}\right) + \left(\frac{u_y}{u_1}\right)\left(\frac{B_z}{B_1}\right)\right] \tag{8}$$

$$\frac{d}{d(\Omega_{ci}\tau)}\left(\frac{u_y}{u_1}\right) = \left[\left(\frac{\gamma}{\gamma_1}\right) - \left(\frac{u_x}{u_1}\right)\left(\frac{B_z}{B_1}\right)\right], \tag{9}$$

where τ is the proper time, u_1 is the upstream 4–velocity, $\Omega_{ci} \equiv ZeB_1/(Am_p c)$, $r_{Li} \equiv u_1/\Omega_{ci}$, and $E_1 \equiv \beta_1 B_1$.

The fields must satisfy Maxwell's equations including the charge and current densities of the pairs in the source terms. One can show that when the upstream ion flow energy dominates that of the pairs, $1/\sigma_i \gg 1/\sigma_\pm$, these are well represented by bulk $\boldsymbol{E} \times \boldsymbol{B}$ drift of the charged pair fluid, and the field equations take the form

$$\frac{d}{d(x/r_{Li})}\left(\frac{E_x}{E_1}\right) = \frac{1}{\sigma_i}\left[\sum \frac{\beta_1 \gamma}{|u_x|} - \left(\frac{B_z}{B_1}\right)\right] \tag{10}$$

$$\frac{d}{d(x/r_{Li})}\left(\frac{B_z}{B_1}\right) = -\frac{\beta_1^2}{\sigma_i}\left[\sum \frac{u_y}{|u_x|} - \left(\frac{E_x}{E_1}\right)\right]. \tag{11}$$

For the parameter ranges of interest, it turns out that the soliton structure must include ion reflection, like the solutions found by Alsop and Arons (1988) for the symmetric, pure pairs soliton. The sums in equations (10-11) are over incoming, reflected, and outgoing ion contributions. Solutions to equations (7-11) are obtained by an iterative method, starting with a guess for the fields and gradually improving it by recursively solving equations (7-9) and (10-11).

Figure 4 displays the soliton for the parameters of the shock simulation shown in Figure 1. The soliton can be seen to represent adequately the initial reflected ion

loop and its associated magnetic overshoot; a correct representation of subsequent overshoots, however, may require the inclusion of some model of ion energy dissipation. After incorporating the effects of the spherically divergent wind geometry and of Doppler beaming and boosting due to the mildly relativistic bulk motion of the synchrotron-emitting pairs, we should be in a position to fit the observed brightness profile of the wisps as a function of the wind parameters.

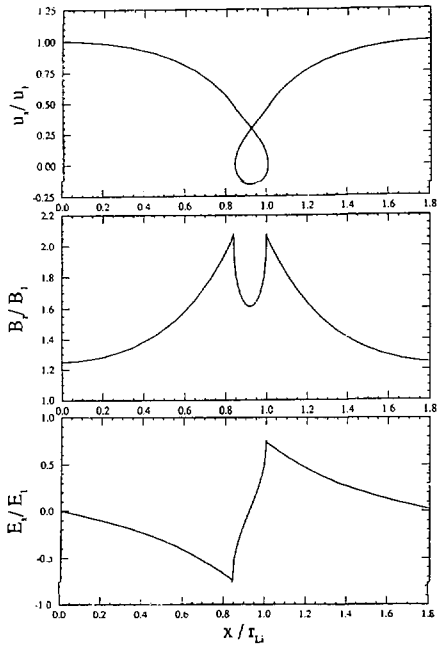

Fig. 4 — "Soliton" with $1/\sigma_i = 2$, $1/\sigma_\pm \approx 0.9$, and $\gamma_1 = 40$. Top panel shows the ion orbits in u_x vs x form, while middle and lower panels respectively show the magnetic and electrostatic fields. The reflected ion orbit, doubly peaked magnetic field overshoot, and symmetrically peaked electrostatic field can clearly be recognized as the leading structure of the shock in Figure 1.

A model of the evolution of the pairs' energy distribution, now being developed, that accounts for the pairs' acceleration through a combination of resonant absorption of collective ion cyclotron waves and magnetic pumping in the overshoot structure given by the soliton model, should then provide quantitative predictions about the spectrum of the synchrotron emission from the wisps. A longer-term prospect is that current investigations of the nature and efficiency of the pair isotropization mechanism (Yang *et al.* 1992) will make it possible to construct complete synthetic brightness maps of the wind shock region, including its azimuthal structure, to be confronted with the full two-dimensional image.

5 MODEL PREDICTIONS: SPECTRUM AND VARIABILITY

The relativistic shock structure model makes potentially testable predictions about the spectrum and variability of the wisps, which will be put forth qualitatively here. The wind parameter fitting outlined above, once completed, should allaw us to make more quantitative the predictions concerning the wisps' spectrum. The first wisp is expected to have a spectrum close to *Maxwellian* synchrotron (*e.g.* Jones and Hardee 1979), with flux $F_\nu \propto \nu^{1/3}$ roughly up to the thermal critical frequency [eq. (3)] and decreasing rapidly with higher frequencies. With increasing distance behind the shock, and thus with increasing wisp number, the high-frequency part of the spectrum should evolve toward a nonthermal power-law form, as the synchrotron-emitting pairs are gradually accelerated to an energy distribution of the Maxwellian plus power-law type (Hoshino *et al.* 1992).

The other major application of the model concerns the variation of the wisps' position with time. Our shock simulations show that for weakly magnetized flows, shock propagation is intrinsically unsteady, and proceeds in a series "jumps" of the initial reflected loop by distances of order the ion Larmor radius, $r_{\rm Li}$, on time scales of order the corresponding gyrofrequency. Thus we expect the position of the wisps to vary on time scales of several months, independently of any fluctuations in the outflow from the pulsar. Such variability has indeed been documented by Scargle (1969), although the time resolution between his observations was insufficient to determine the exact behavior of the wisps as a function of time. Earlier observations by Baade suggested that the main wisp forms and slowly moves downstream, eventually to be replaced by a new main wisp (Oort and Walraven 1956). This behavior would be consistent, for a weakly magnetized wind, with shock propagation as observed in our simulations. More quantitative predictions about the time-variable behavior will probably become accessible, via some form of simulation, once the basic parameters of the wind are better constrained by fitting the time-stationary average structure.

6 SUMMARY AND PROPAGANDA

We argue that the structure of the collisionless shock terminating the relativistic wind from the Crab pulsar should be observationally resolvable, and we suggest the identification of the wisps with synchrotron emission from this shock structure. The observed length scale, morphology and energetics of the wisps all support this interpretation, and the time variability of the wisps' position is also consistent with this picture. The main test of the model will lie in the predicted spectrum of the wisps'continuum emission, which was described qualitatively above, and which modelling in progress should allow us to study more quantitatively. Clearly, modern observations on the spectrum and time-variability of the wisps, in the IR, optical, UV and X-ray wavebands, would prove extremely interesting.

In a meeting largely devoted to high-energy emission from pulsars, it is perhaps not inappropriate to stress that of all the observable manifestations of pulsars, the largest fraction by far of the total spindown luminosity is invested into pulsar winds. Thus relativistic winds are the most important "emission mechanism" to be accounted for by pulsar magnetospheric theory, and the inferences about the pulsar wind parameters and composition expected from our current work should provide detailed observational constraints on this question.

ACKNOWLEDGEMENTS

We wish to express our gratitude to S. van den Bergh and C. Pritchet for allowing us to use their CCD image of the Crab Nebula's wisps. The research described here was supported in part by NSF grant AST-9115093 and by IGPP-LLNL grant 92-93, and was performed in part under the auspices of the DOE at LLNL under contract W-7405-Eng-48.

REFERENCES

Alsop, D., and Arons, J. 1988, *Phys. Fluids*, **31**, 839.
Aschenbach, B., and Brinkmann, W. 1975, *Astr. Ap.*, **41**, 147.
Brinkmann, W., Aschenbach, B., and Langmeier, A. 1985, *Nature*, **313**, 662.
Emmering, R. T., and Chevalier, R. A. 1987, *Ap. J.*, **321**, 334.
Gallant, Y. A., Hoshino, M., Langdon, A. B., Arons, J., and Max, C. E. 1992, *Ap. J.*, **391**, in press.
Helfand, D. J., and Becker, R. H. 1987, *Ap. J.*, **314**, 203.
Hoshino, M., and Arons, J. 1991, *Phys. Fluids B*, **3**, 818.
Hoshino, M., Arons, J., Gallant, Y.A., and Langdon, A.B. 1992, *Ap. J.*, **389**, in press.
Jones, T. W., and Hardee, P. E. 1979, *Ap. J.*, **228**, 268.
Kennel, C. F., and Coroniti, F. V. 1984a, *Ap. J.*, **283**, 694.
Kennel, C. F., and Coroniti, F. V. 1984b, *Ap. J.*, **283**, 710.
Kundt, W., and Krotscheck, E. 1980, *Astr. Ap.*, **83**, 1.
Lampland, C. O. 1921, *Pub. A. S. P.*, **33**, 79.
Michel, F. C., Scowen, P. A., Dufour, R. J., and Hester, J. J. 1990, *Ap. J.*, **368**, 463.
Oort, J. H., and Walraven, Th. 1956, *Bull. Astr. Inst. Netherlands*, **12**, 285.
Rees, M. J., and Gunn, J. E. 1974, *M.N.R.A.S.*, **167**, 1.
Scargle, J. D. 1969, *Ap. J.*, **156**, 401.
van den Bergh, S., and Pritchet, C. J. 1989, *Ap. J. (Letters)*, **338**, L69.
Weiler, K. W. 1985, in *The Crab Nebula and Related Supernova Remnants*, ed. M. C. Kafatos and R. B. C. Henry (Cambridge: Cambridge University Press), p. 265.
Weiler, K. W., and Sramek, R. A. 1988, *Ann. Rev. Astr. Ap.*, **26**, 295.
Yang, T.-Y. B., Gallant, Y. A., Arons, J., and Langdon, A. B. 1992, in preparation.